

Citation for published version:

Litherland, AGM, Spurway, LM, Gordeev, SN, Aaronson, BDB, Wain, AJ, O'Connell, MA, Piili, H, Hovilehto, M, Matilainen, VP, Vuorema, A & Marken, F 2018, 'Galvanic exchange platinization reveals laser-inscribed pattern in 3D-LAM-printed steel', Journal of Solid State Electrochemistry, vol. 22, no. 6, pp. 1-8.
<https://doi.org/10.1007/s10008-017-3869-8>

DOI:

[10.1007/s10008-017-3869-8](https://doi.org/10.1007/s10008-017-3869-8)

Publication date:

2018

Document Version

Peer reviewed version

[Link to publication](#)

Publisher Rights

CC BY

University of Bath

General rights

Copyright and moral rights for the publications made accessible in the public portal are retained by the authors and/or other copyright owners and it is a condition of accessing publications that users recognise and abide by the legal requirements associated with these rights.

Take down policy

If you believe that this document breaches copyright please contact us providing details, and we will remove access to the work immediately and investigate your claim.

REVISION 2

12th December 2017

Galvanic Exchange Platinisation Reveals Laser-Inscribed Pattern in 3D-LAM-Printed Steel

Alex G.M. Litherland ¹, Lee M. Spurway ¹, Sergey N. Gordeev ¹, Barak D.B. Aaronson ², Andrew J. Wain ³, Michael A. O'Connell ³, Heidi Piili ⁴, Mikko Hovilehto ⁴, Ville-Pekka Matilainen ⁴, Anne Vuorema ⁵, Frank Marken*²

¹ *Department of Physics, University of Bath, Claverton Down, Bath BA2 7AY, UK*

² *Department of Chemistry, University of Bath, Claverton Down, Bath BA2 7AY, UK*

³ *National Physical Laboratory, Teddington, United Kingdom, TW11 0LW, UK*

⁴ *Laser Processing Research Group, Lappeenranta University of Technology, Tuuantokatu 2, 53850 LPR Lappeenranta, Finland*

⁵ *LUT RE-SOURCE Research Platform, Lappeenranta University of Technology, Skinnarilankatu 34, 53850 Lappeenranta, Finland*

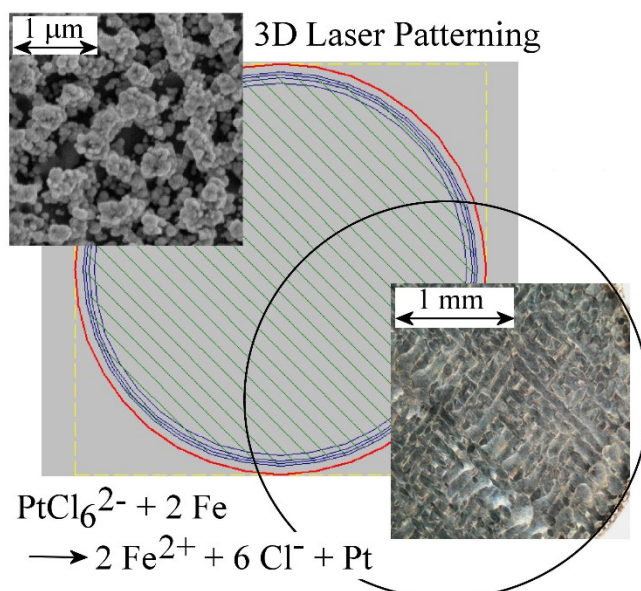
To be submitted to Journal of Solid State Electrochemistry

Proofs to F. Marken (f.marken@bath.ac.uk)

Abstract

Galvanic exchange involving dissolution of iron and the simultaneous growth of platinum onto 316L stainless steel was investigated for specimens manufactured by 3D-printing, and the behaviour was compared to conventional stainless steel. Novel phenomena associated with the 3D-printed steel, but not conventional steel, reacting in three distinct phases were observed: first, with low platinum loading a bright etching pattern linked to the laser-manufacturing process is revealed at the steel surface; second, a nanostructured pore pattern with platinum nano-deposits forms; and third, a darker platinum film coating of typically 500 nm thickness forms and then peels off the steel surface with further platinum growth underneath. Unlike the conventional steel (and mainly due to residual porosity), 3D-printed steel supports well-adhered platinum films for potential application in electro-catalysis, as demonstrated for alkaline methanol oxidation.

Graphical Abstract



Keywords: laser pattern; electroless deposition; nanoporosity; catalysis; alloys.

1. Introduction

Three dimensional printing, although invented around thirty years ago, is still a method in its infancy in terms of delivering novel research materials [1]. There are many 3D-printing technologies [2], a common approach being powder bed fusion or “laser additive manufacturing” (LAM) wherein layers of material are stacked and laser-melted on top of each other, to erect a three dimensional construct [3]. 3D-printing has revolutionized some areas of industry and the continued development of this technique has led to a dramatic rise in associated publications in recent years [4,5]. The properties of 3D-printed metal objects can differ from those fabricated with subtractive manufacturing techniques and therefore it is reasonable to investigate these new materials and to compare them to their conventional counterparts. Here, differences in the electrochemical properties for conventional 316L steel and 3D-printed steel are studied.

A wide range of applications for 3D-printed materials have been proposed, including in chemical reaction-ware [6], in microfluidics [7], and in electrochemistry [8,9]. 3D-printed steel has been suggested for helical electrodes in electrolyzers [10], and for fuel cell components [11]. Like conventional steel, the surface of 3D-printed steel is typically covered with a protective oxide layer, but this can be breached in aqueous HCl media, resulting in hydrogen evolution or metal dissolution and/or deposition processes. Recently, we have shown that 3D-printed steel surfaces are readily modified with platinum catalysts in a simple galvanic exchange process [12]. Compared to other types of platinum deposition (sputtering [13], focused ion beam deposition [14], thermolytic deposition [15], or atomic layer deposition [16]) galvanic exchange is practical and efficient [17]. When testing the electrodes produced by galvanic exchange platinisation, it was observed that the electrocatalytic performance towards methanol oxidation (in acidic media) was improved relative to that for similar platinum nano-materials. The effect was attributed to iron (and possibly other) impurities becoming incorporated into the galvanically exchanged platinum catalyst to promote the catalytic activity [12,18,19].

Here, the galvanic exchange platinisation for 2 mM PtCl_6^{2-} in aqueous 1 M HCl is investigated in more depth and compared for conventional steel and 3D-printed steel. It is shown that 3D-printed steel shows a remarkable reactivity pattern (with laser-aided manufacturing pattern inscribed in the material being revealed) distinctly different from that for conventional steel.

Three stages of galvanic exchange platinum deposition can be distinguished, which are linked to a micro-pattern formation (associated with the laser inscribed printing pattern of typically 100 μm feature size), nano-pattern formation at 50 nm scale, and finally platinum film overgrowth (typically 500 nm thick) and peel-off. These processes are observed only on 3D-printed steel and there are no similarly defined processes observed on conventional steel surfaces. The origin of this behaviour is explored and potential for applications in electro-catalysis in alkaline media is discussed.

2. Experimental

2.1. Reagents, Instrumentation, and Materials

Reagents such as HCl (35%), KOH (A.R.), methanol (chromatography grade), and hexachloroplatinic acid were obtained from Sigma-Aldrich or Johnson Matthey Ltd. and used without further purification. Water (demineralised and filtered) was taken with not less than 18.2 M Ω cm (at 293 K) from a Thermo Scientific water purification system. Experiments were performed at 20 \pm 2 $^{\circ}\text{C}$.

For scanning electron microscopy (SEM) imaging on a JEOL JSM6310 instrument, the potential difference was set between 5-15 kV to achieve good resolution. Energy dispersive x-ray spectroscopy (EDX) was used for chemical analysis using a Zeiss Supra SEM equipped with an Oxford Instruments X-Man Detector.

Conventional 316L steel rods of 3 mm diameter were purchased from Advent Research materials Ltd. The 3D-printed steel rods were prepared from SS 316L powder (EOS GmbH - Electro Optical Systems, Robert-Stirling-Ring 1, D-82152 Krailling, München) at Lappeenranta University of Technology in Finland as reported previously [12]. Briefly, a powder of steel with typically 20 μm diameter is layered over the sample surface and then laser sintered. The laser passes over the surface in a line pattern (with 100 μm distance between lines) with each layer being sintered at a 90 degree angle relative to the previous (see Figure 1A).

2.2. Preparation of Steel Disks

The 3 mm diameter steel rods (conventional and 3D-printed) were then cut into disks of typically 1 mm thickness and polished to mirror finish (see Figure 1B and 1C). Abrasives used to hand-polish were P800 emery paper with a grain size of 22 μm , diamond pastes with reduced grain sizes 15 μm , 6 μm , and 1 μm (obtained from Metprep and Joke[®]-Hyprez[®] respectively) and finally Linde[™] high purity 0.3 μm Micron Type A alumina powder. In between each phase of polishing it was paramount that the disks were cleaned effectively. This was achieved by cleaning the samples with a brush, ultrasonicing in deionized water, and then by rinsing with isopropanol. Some residual porosity in the steel samples is observed in particular for the conventional steel (Figure 1C). The elemental composition as obtained by energy-dispersive X-ray analysis (EDX) is summarized in Table 1. We note that the composition of the 3D-printed steel is not identical to that of conventional 316, but exhibit small differences, particularly in the Nickel and Molybdenum content, which may impact the corrosion behavior of the material. A DP-M17 USB Digital Microscope from Conrad Electronics with a magnification of 200 \times was used to optically monitor the polishing process. The samples were polished to a surface roughness average of ~ 6 nm (over $10\ \mu\text{m} \times 10\ \mu\text{m}$; measured by AFM).

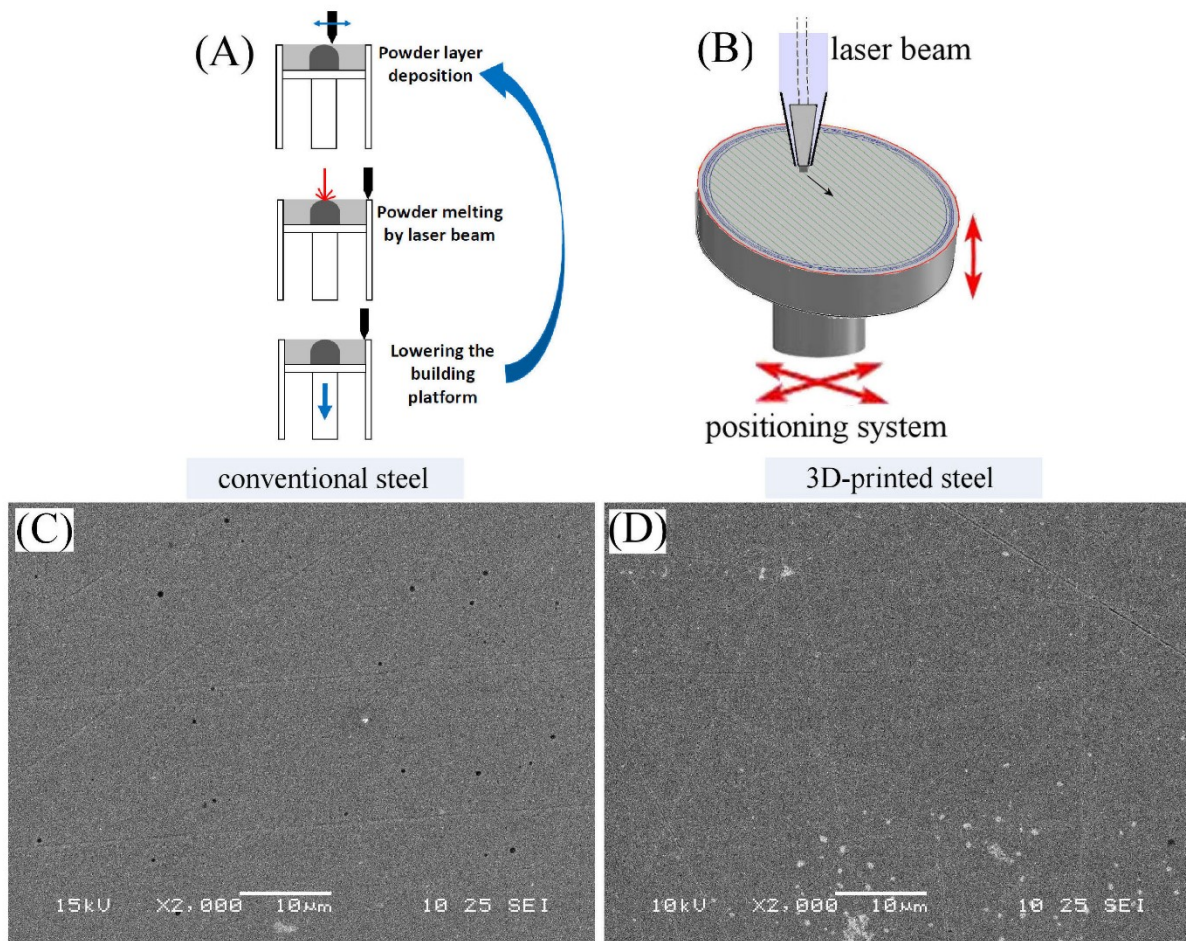


Figure 1. (A) Schematic depiction of the 3D-printing process. (B) Diagram showing the laser melting following a line pattern. The laser spot is approximately 100 μm in diameter and the distance between consecutive lines is 100 μm . In consecutive layers the line pattern is rotated by 90 degrees. (C,D) Scanning electron micrographs (SEM) for (C) a conventional steel sample and (D) a 3D-printed steel sample after polishing.

Table 1. Chemical composition for the five most abundant elements for 316L samples for 3D-printed material and for conventional steel obtained using EDX analysis.

Elements	316L (3D-printed)	316L (conventional)
Iron	$61.6 \pm 0.4\%$	$66.6 \pm 0.1\%$
Chromium	$17.9 \pm 0.1\%$	$17.3 \pm 0.1\%$
Nickel	$13.5 \pm 0.1\%$	$10.2 \pm 0.1\%$
Molybdenum	$3.0 \pm 0.1\%$	$2.3 \pm 0.1\%$
Manganese	$1.3 \pm 0.1\%$	$1.5 \pm 0.1\%$

2.3. Galvanic Exchange Platinisation Experiments

Platinum was grown *via* a galvanic exchange process, by immersion into a solution of 2 mM PtCl_6^{2-} (hexachloroplatinic acid from Johnson Matthey Ltd.) in aqueous 1 M HCl. Steel samples were immersed for periods of 30 s, 1 minute, 2 minutes, 5 minutes, or 15 minutes under ambient conditions. After deposition, samples were rinsed with distilled water and dried in a flow of nitrogen gas.

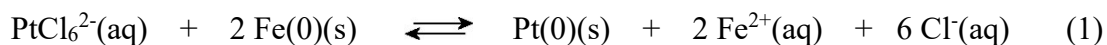
2.4. Electrochemical Experiments

Steel rods with a length of 9 mm were sealed in silicone (Silicoset 150) to expose a 3 mm diameter disk surface. Chronopotentiometry and cyclic voltammetry measurements were performed using a microAutolab III potentiostat (EcoChemie, NL) with GPES control software. A conventional three-electrode cell with saturated calomel (SCE) reference and platinum wire counter electrode was employed. Electrolyte solutions were not de-aerated or stirred during electrochemical measurements.

3. Results and Discussion

3.1. Comparison of Galvanic Exchange Reactivity of Conventional and 3D-Printed Steel

It has recently been shown [12] that platinum catalyst coatings are formed on both conventional steel (with poor adhesion) and 3D-printed steel (with good adhesion) when exposed to a solution of PtCl_6^{2-} in aqueous HCl. The process is consistent with galvanic exchange [20] and formally expressed in equation 1. This process should be equally possible on both conventional and 3D-printed steel, but characteristic differences were observed when comparing the two types of steel.



Although equation 1 appears relatively simple, there are reaction intermediates such as Pt(II) and other reactive metals present in stainless steel (see Table 1) are likely to lead to more complex reaction conditions. Figure 2A shows chronopotentiometry data for a 3 mm diameter disk sample of conventional steel compared to the case of 3D printed steel immersed in aqueous, aerated, 1 M HCl. In both cases the potential becomes increasingly negative initially upon immersion before approaching an equilibrium value, consistent with dissolution of the air-formed surface film followed by re-passivation. The transient behaviour at short timescales

appears to differ between the two materials, with the conventional steel potential initially “over-shooting” towards more negative values, indicating a difference in the relative rates of passive film dissolution and re-passivation. This disparity likely relates to the intrinsic corrosion properties of the two materials, but differences in the precise surface state and the influence of residual stress cannot be ruled out.

When these experiments were repeated in 1 M HCl with added 2 mM PtCl_6^{2-} (see Figure 2B), generally more positive potentials are observed consistent with a faster dissolution of the steel during galvanic exchange. This is likely to be linked to the deposition of platinum onto the steel surface, which acts to inhibit passive film formation by blocking active sites. Optically, the formation of platinum metal deposits is seen for both conventional steel and 3D-printed steel, but the types of deposits appear to be different.

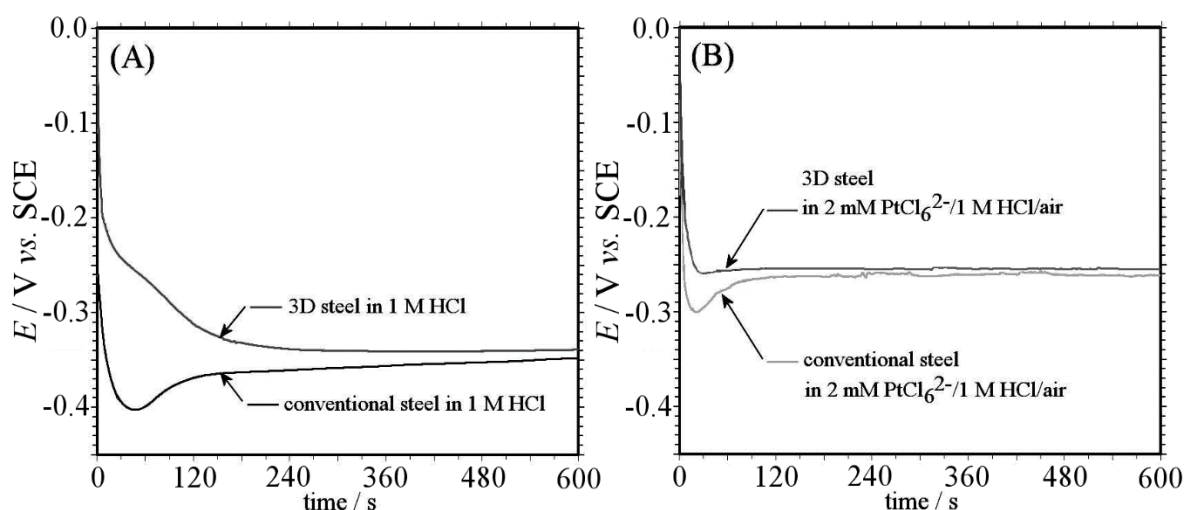


Figure 2. (A) Chronopotentiometry data for 3 mm diameter disk samples of conventional steel and 3D-printed steel immersed in aqueous 1 M HCl. (B) Chronopotentiometry data for 3 mm diameter disk samples of conventional steel and 3D-printed steel in 1 M HCl containing 2 mM PtCl_6^{2-} .

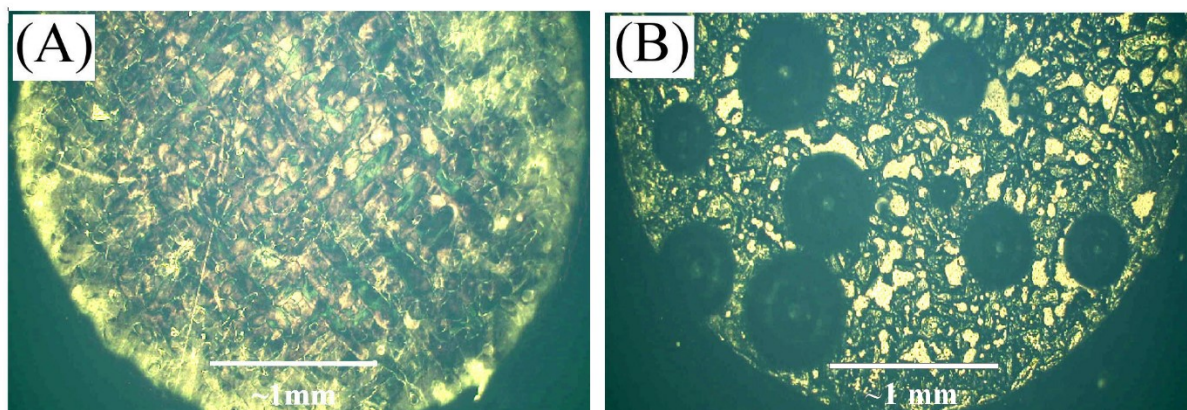


Figure 3. Optical micrographs (obtained *in situ*) showing the difference in hydrogen evolution characteristics for (A) 3D-printed steel and (B) conventional steel immersed for 90 s in 2 mM PtCl_6^{2-} in 1 M HCl.

When studied with *in situ* optical microscopy, upon immersion in aqueous 2 mM PtCl_6^{2-} in 1 M HCl, the 3D-printed steel appeared to develop a pattern of lines during the galvanic exchange (see Figure 3A). In contrast, the conventional steel sample appeared to be more active towards production of hydrogen bubbles, consistent with the more negative potentials observed upon exposure to this galvanic exchange solution (see Figure 2).

Exposing samples to the galvanic exchange solution for different lengths of time (1 minute, 2 minutes and 5 minutes) unveiled further differences in the behaviour of the two types of steel. Platinum growth appeared to initiate more quickly on the conventional steel sample (see Figure 4A). After 1 minute of immersion the surface of the conventional steel sample turns dark and a deposit is clearly observed. Over longer periods of time platinum appears to form in a random pattern and with weak adhesion (Figures 4B and 4C). In contrast, for the 3D-printed steel, initially a unique “domain” pattern was observed (Figure 4D). Rectangular regions with approximately 100 μm width with a right angle pattern are seen after 1 minute immersion. This pattern appears to closely resemble the laser-scanning pattern applied during the 3D-printing process, in which the laser is scanned in a line pattern with a 100 mm period, which is rotated by 90 degrees after each layer. A possible explanation for the observed behaviour is dendritic growth of the 3D-printed material leading to non-uniform elemental distribution within individual grains, and thus a spatially varied susceptibility to localised corrosion. Whilst this

non-uniformity was not evident from energy-dispersive x-ray (EDX) mapping experiments, the minimum difference in composition required to bring about a change in electrochemical behaviour is likely beyond the sensitivity of this technique. An alternative mechanism could be spatial differences in the residual stress within the steel microstructure, again arising from the 3D-printing process, but further work would be required to investigate this phenomenon.

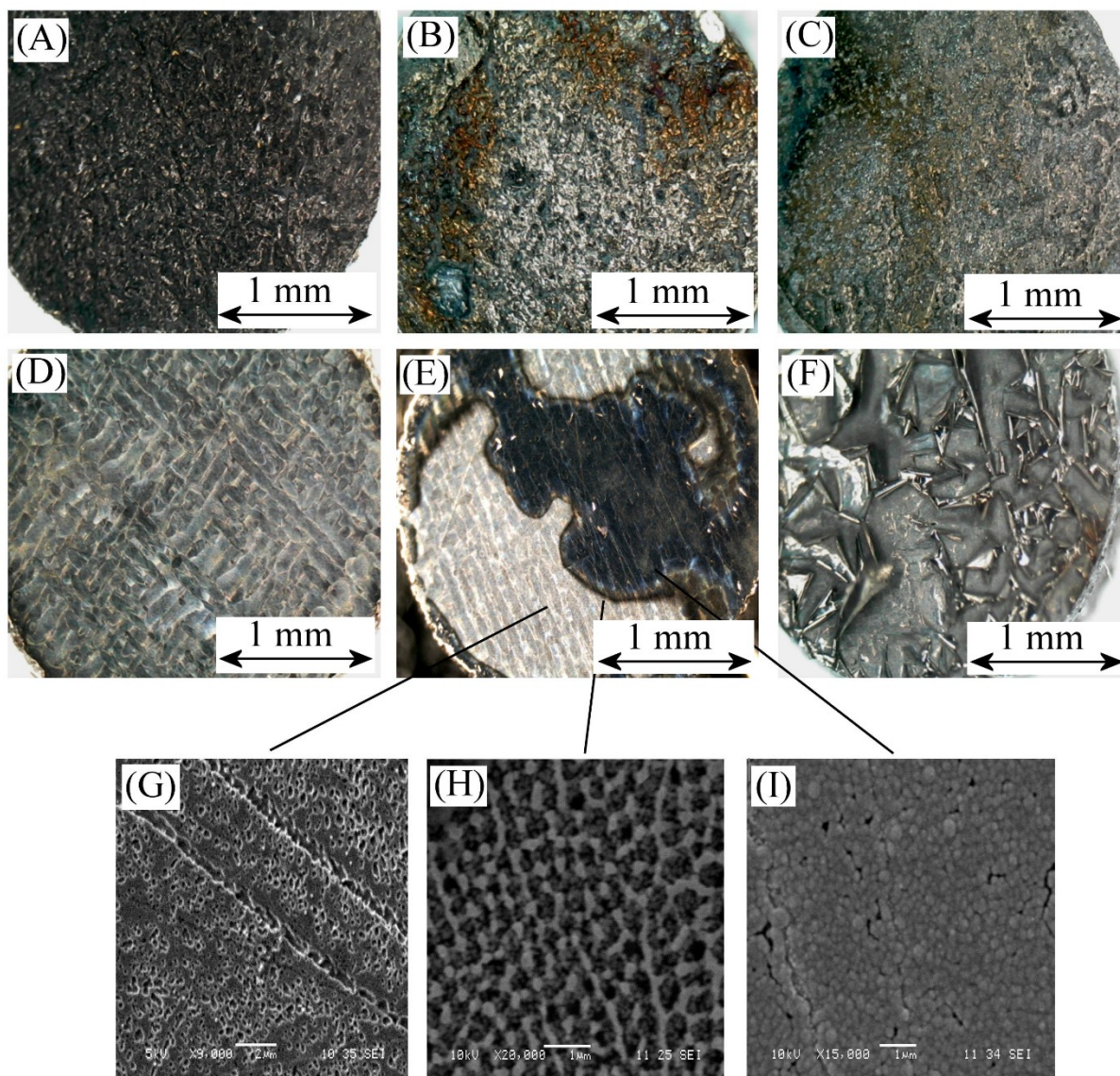


Figure 4. (A-F) Optical micrographs recorded after immersion in 2 mM PtCl_6^{2-} in 1 M HCl for conventional steel (A-C, top row) and for 3D-printed steel (D-F, bottom row). The immersion time was 1 minute (A and D), 2 minutes (B and E), and 5 minutes (C and F). (G-I) Scanning electron microscopy (SEM) images for (G) the bright region, (H) the border region, and (I) the dark region shown in 4E.

With time the 3D-printed steel sample then developed a black coloration (starting from the edges and then covering the complete surface, Figure 4E) before large flakes of platinum appear (Figure 4F) to delaminate from the steel surface. It is clear from these observations (which were consistent across multiple experiments) that the galvanic exchange behaviour of these two materials differs considerably.

An optical microscopy comparison of the properties of conventional steel and 3D-printed steel after a simple etch treatment in 1 M HCl did not reveal any differences. Also, scanning electron microscopy (SEM) and EDX analysis, revealed no significant differences seen for the two types of steel sample. Only under galvanic exchange conditions are differences in reactivity and the laser line pattern exposed.

3.2. Galvanic Exchange Platinum Growth on 3D-Printed Steel

Analysis of the 3D-printed steel sample exposed for 2 minutes to galvanic exchange conditions, reveals three distinct regions to explore. Figures 4G to 4I show typical SEM images for the brighter region (Figure 4G), the interface between the dark and bright regions (Figure 4H), and the dark region (Figure 4I). In the brighter region only insignificant amounts of platinum are present (measured by EDX) and corrosion products such as oxides seem to dominate. The SEM image (Figure 4G) indicates that the surface is heavily corroded, with the highest density of pits or localised corrosion concentrated along distinct lines, consistent with non-uniformities in the 3D-printing process leading to regions of higher susceptibility to corrosion, as discussed above. In the dark region layers of platinum are clearly present. These are formed from individual nanoparticles that merge into a single layer (Figure 4I). This layer appears to densify and then lifts off the steel surface in large flakes (see Figure 4F). Very interesting is the boundary layer where regular sub-micron patterns of platinum and oxide are present (Figure 4H).

SEM images for the platinum flakes that form after 5 minutes galvanic exchange are shown in Figures 5A and 5B. These platinum flakes consist of individual nanoparticles that have grown together to form approximately 500 nm thick films. Due to continuing corrosion at the passive oxide surface of the steel underneath the platinum film, cracks appear and delamination of the film is observed.

Interestingly, SEM imaging of the boundary between the lighter and darker areas revealed a nanoporous etching pattern with platinum deposits (confirmed by EDX) growing inside (Figure 5C and D). This pattern appears to suggest a well-distributed platinum deposit in the form of “nano-cages” with enhanced surface area. For applications in electrocatalysis this type of surface may be of particular interest.

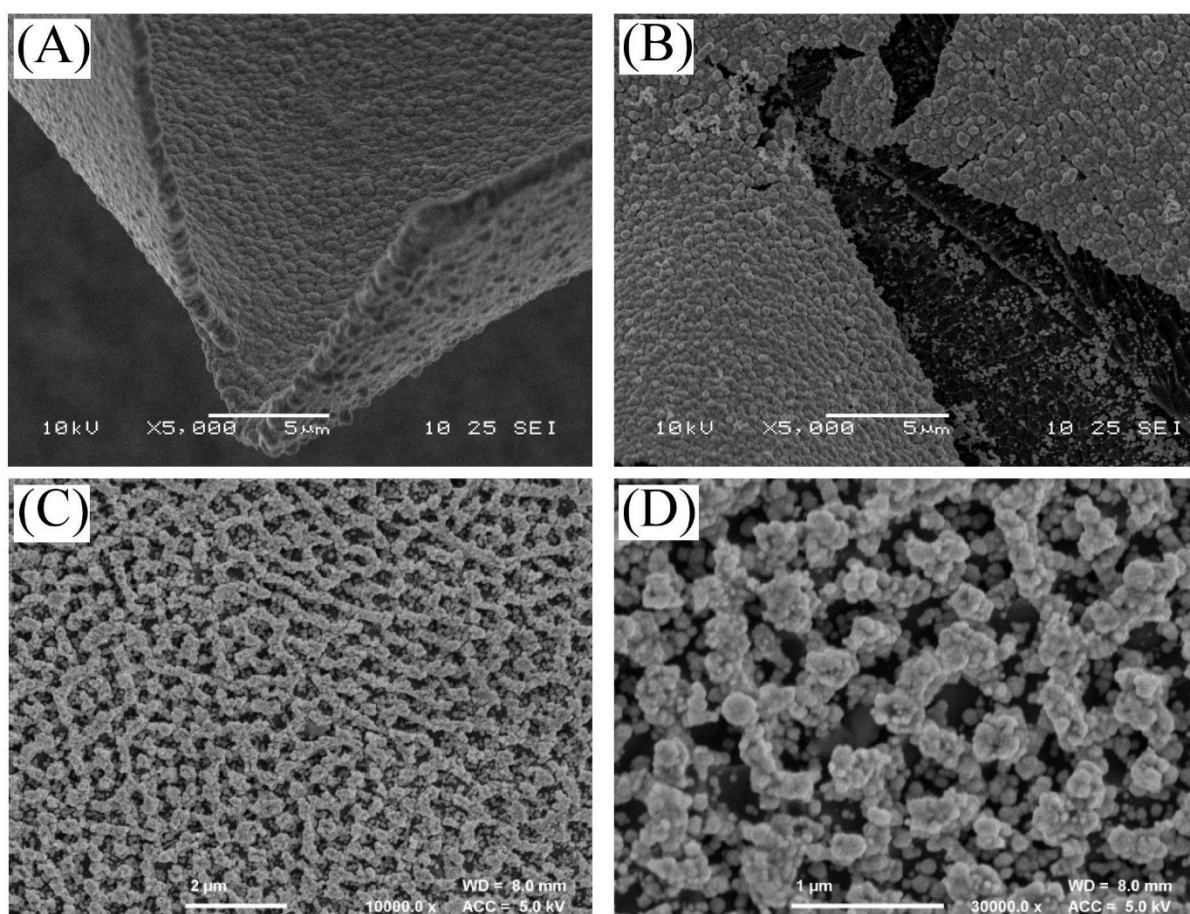


Figure 5. SEM images (A) and (B) of a platinum peel on the 3D-printed steel sample after 5 minutes galvanic exchange. Also shown are SEM images (C) and (D) for 2 minutes galvanic exchange obtained in the boundary layer.

Another phenomenon was observed for galvanic exchange on the 3D-printed steel when using a lower concentration (1 mM) of PtCl_6^{2-} in 1 M HCl solution. For the conventional steel a

similar deposition process occurred to that shown in Figure 4A-C, although the rate of the deposition process appeared approximately half as fast. For the 3D-printed steel only etching was observed to occur and no platinum layer formed when using 1 mM PtCl_6^{2-} solution, even after 15 minutes reaction time. This implies that there could be a concentration threshold for PtCl_6^{2-} galvanic exchange, below which platinum deposition is not favoured on the 3D-printed steel.

3.3. Electrocatalytic Activity of Galvanic Exchange Platinum on Conventional Steel *versus* 3D-Printed Steel

Next, in preliminary electrocatalysis test experiments, the behaviour of both the conventional steel and 3D-printed steel after 2 minutes galvanic exchange deposition of platinum are compared in terms of reactivity towards methanol oxidation in aqueous 1 M KOH. The 2 minute galvanic exchange deposition of platinum was chosen to explore reactivity of the nano-patterned surface (Figure 5C and 5D). It has recently been proposed that much more substantial platinum deposits on 3D-printed steel show promising reactivity [12].

Figure 6A shows current density data (experimental data was scaled to 1 cm² geometric surface area) for cyclic voltammograms obtained at a scan rate of 50 mVs⁻¹. Whilst no catalytic response towards methanol is observed on native steel electrodes, in the presence of deposited platinum a characteristic anodic peak is observed at approximately -0.3 V *vs.* SCE. Recent studies on galvanically exchanged platinum catalysts on other types of metal surfaces have shown very similar results for methanol oxidation in alkaline media [21]. The oxidation process at this potential can be assigned to methanol oxidation (equation 2), which is of particular relevance to fuel cell applications [22,23].

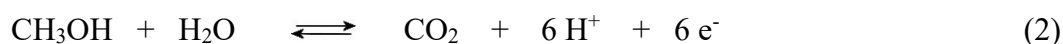


Figure 6A shows the methanol oxidation behaviour for three types of electrode: platinum deposited on 3D-printed steel, platinum deposited on conventional steel, and a polycrystalline platinum disk for comparison. Although currently no detailed information on the true platinum loading or platinum surface area can be provided, it is apparent that the magnitudes of the peak current densities differ considerably, with conventional steel exhibiting the lowest currents,

probably due to poor adhesion of the galvanically exchanged platinum catalyst. The 3D-printed steel sample exhibited the highest current densities (one order of magnitude higher than a bare platinum surface) presumably due to a high surface area and nano-structuring of the platinum deposit (Figure 6B). A further observation can be made in terms of the onset potential for the electrocatalytic methanol oxidation. For both the forward and the reverse potential scan the onset potential for methanol oxidation is lower by approximately 0.2 V for the 3D-printed steel coated with platinum compared to the other platinum electrodes. This observation supports our previous hypothesis [12] that platinum deposited by galvanic exchange onto 3D-printed steel exhibits a superior catalytic activity, potentially due to trace contamination from steel metals (mainly iron). The role of iron “impurities” in methanol fuel cell catalysis has been highlighted by Antolini [19]. More work will be required to further explore the feasibility of these steel-platinum electrodes in fuel cell systems in terms of durability and stability against corrosion and loss of activity.

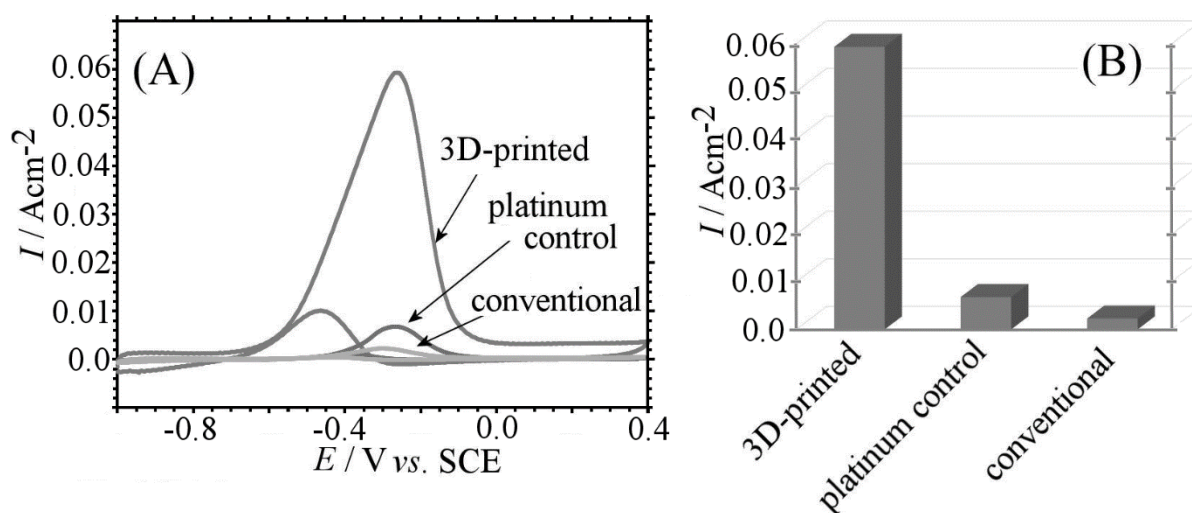


Figure 6. (A) Cyclic voltammetry data (scan rate 50 mVs⁻¹) for a conventional steel electrode and a 3D-printed steel electrode (both with 2 minutes galvanic exchange deposited platinum) as well as a polycrystalline platinum disc electrode immersed in 1.5 M methanol in aqueous 1 M KOH. (B) Bar chart comparing the current density of the peak for methanol oxidation at the three different electrode materials.

4. Conclusions

In this paper we have demonstrated dramatic differences in the electrochemical behavior of conventional and 3D-printed steel with respect to a galvanic platinum exchange process. The differences in reactivity relate back to the production method and in particular the laser-annealing process leaving a pattern of residual porosity. The growth of platinum on 3D-printed steel occurs in three distinct stages. The first stage is associated with steel passivation and corrosion, which results in a bright pattern of pits and localized corrosion linked to the laser melting process. Uniquely, this “laser inscription” is only revealed under galvanic exchange conditions, indicating that PtCl_6^{2-} plays an important role in highlighting spatial non-uniformities in surface electrochemistry. The origin of this behaviour is unclear but it possibly relates to non-uniform elemental distribution within the alloy leading to “tracks” of higher and lower susceptibility towards corrosion. As the sample continues to corrode, a darker region is formed with platinum deposition taking place and a region of nanoporous platinum forming at the interface. Finally, micron-thick layers of nanoparticulate platinum form with black appearance. When this last stage is reached, the layer begins to delaminate from the surface while remaining attached, revealing the exposed steel, upon which platinum continues to grow. The platinum deposited on 3D-printed steel shows much improved adhesion compared to that grown on conventional steel, which does not exhibit any evidence of spatial patterning.

Exploratory electrocatalysis experiments focusing on methanol oxidation in alkaline media suggest improved catalytic performance for the 3D-printed steel after galvanic exchange as indicated by lower onset potentials and significantly enhanced current densities compared to platinum deposited on conventional steel. It can be concluded that the 3D-printing process details (laser scanning methods and pattern) can significantly affect applications in electrocatalysis. Further work will be required to reveal more structural details for the galvanically deposited platinum. There are a range of other applications with other alloys where the 3D-printing approach followed by galvanic exchange could be of interest. Finally, the visualization of laser-inscribed pattern could be of interest in other areas of such as steel product recognition.

Acknowledgements

B.D.B.A. is grateful for support from the Leverhulme Foundation (RPG-2014-308: “New Materials for Ionic Diodes and Ionic Photodiodes”). AJW and MAO’C thank the UK National Measurement System (Department of Business, Energy & Industrial Strategy) for financial support.

References

-
- [1] Gross BC, Erkal JL, Lockwood SY, Chen C, Spence DM (2014) Evaluation of 3D printing and its potential impact on biotechnology and the chemical sciences. *Anal Chem* 86: 3240–3253
 - [2] Costa L, Vilar R (2009) Laser powder deposition. *Rapid Prototyping J* 15: 264–279
 - [3] Ambrosi A, Pumera M (2016) 3D-printing technologies for electrochemical applications. *Chem Soc Rev* 45: 2740–2755
 - [4] Schubert C, van Langeveld MC, Donoso LA (2014) Innovations in 3D printing: a 3D overview from optics to organs. *Brit J Ophthalmol* 98: 159–161
 - [5] Lipson H, Kurman M (2013) *Fabricated: the new world of 3D printing*, John Wiley and Sons, Indianapolis, 22–24
 - [6] Symes MD, Kitson PJ, Yan J, Richmond CJ, Cooper GJT, Bowman RW, Vilbrandt T, Cronin L (2012) Integrated 3D-printed reactionware for chemical synthesis and analysis. *Nature Chem* 4: 349–354
 - [7] Erkal JL, Selimovic A, Gross BC, Lockwood SY, Walton EL, McNamara S, Martin RS, Spence DM (2014) 3D printed microfluidic devices with integrated versatile and reusable electrodes. *Lab-on-a-Chip* 14: 2023–2032
 - [8] Fu K, Yao YG, Dai JQ, Hu LB (2017) Progress in 3D printing of carbon materials for energy-related applications. *Adv Mater* 29: UNSP 1603486
 - [9] Rymansaib Z, Iravani P, Emslie E, Medvidovic-Kosanovic M, Sak-Bosnar M, Verdejo R, Marken R (2016) All-polystyrene 3D-printed electrochemical device with embedded carbon nanofiber-graphite-polystyrene composite conductor. *Electroanalysis* 28: 1517–1523
 - [10] Ambrosi A, Moo JGS, Pumera M (2016) Helical 3D-printed metal electrodes as custom-shaped 3D platform for electrochemical devices. *Adv Functional Mater* 26: 698–703

-
- [11] Scotti G, Matilainen V, Kanninen P, Piili H, Salminen A, Kallio T, Franssila S (2014) Laser additive manufacturing of stainless steel micro fuel cells. *J Power Sources* 272: 356–361
 - [12] Weber J, Wain AJ, Piili H, Matilainen VP, Vuorema A, Attard GA, Marken F (2016) Residual porosity of 3D-LAM-printed stainless-steel electrodes allows galvanic exchange platinisation. *ChemElectroChem* 3: 1020–1025
 - [13] Hood C (1976) Coating methods for use with the platinum metals: A review of the available techniques. *Platinum Metals Rev* 20: 48–52
 - [14] Tao T, Ro JS, Melngailis J, Xue Z, Kaesz HD (1990) Focused ion-beam induced deposition of platinum. *J Vac Sci Technol B* 8: 1826–1829
 - [15] Hotchen CE, Attard GA, Bull SD, Marken F (2014) One-step electroless growth of nano-fibrous platinum catalyst from "paint-on" PtCl_6^{2-} solution in poly-(ethylene-glycol). *Electrochim Acta* 137: 484–488
 - [16] Lim BS, Rahtu A, Gordon RG (2003) Atomic layer deposition of transition metals. *Nature Materials* 2: 749–754
 - [17] Ambrozik S, Dimitrov N (2015) The deposition of Pt via electroless surface limited redox replacement. *Electrochim Acta* 169: 248–255
 - [18] Kannan R, Silva AA, Cardoso FM, Gupta G, Aslam Z, Sharma S, Steinberger-Wilckens R (2015) Study of FePt deposited reduced graphene oxide's utility as a catalyst towards oxygen reduction and methanol oxidation reactions. *RSC Adv* 5: 36993–36997
 - [19] Antolini E (2016) Iron-containing platinum-based catalysts as cathode and anode materials for low-temperature acidic fuel cells: a review. *RSC Adv* 6: 3307–3325
 - [20] Alia SM, Yan YS, Pivovar BS (2014) Galvanic displacement as a route to highly active and durable extended surface electrocatalysts. *Catalysis Sci Technol* 4: 3589–3600
 - [21] Hosseini MG, Abdolmaleki M, Esfahlan V (2017) Porous Co/Co-Ni-Pt nanostructures prepared by galvanic replacement towards methanol electro-oxidation. *J Porous Mater* 24: 305–313
 - [22] Lin L, Zhu Q, Xu AW (2015) Anode catalysts and cathode catalysts of direct methanol fuel cells. *Progress Chem* 27: 1147–1157
 - [23] Kumar P, Dutta K, Das S, Kundu PP (2014) An overview of unsolved deficiencies of direct methanol fuel cell technology: factors and parameters affecting its widespread use. *Internat J Energy Res* 38: 1367–1390